Algal Research 41 (2019) 101538

Contents lists available at ScienceDirect

Algal Research

journal homepage: www.elsevier.com/locate/algal

Electrochemical behavior of a composite material containing 3D-structured diatom biosilica

A.P. Nowak[a,*], M. Sprynskyy[b], W. Brzozowska[b], A. Lisowska-Oleksiak[a]

[a] Gdańsk University of Technology, Narutowicza 11/12, 80-233 Gdańsk, Poland
[b] Nicolaus Copernicus University, Gagarina 11, 87-100 Toruń, Poland

A B S T R A C T

3D-structured diatom biosilica mixed with conducting carbon black was investigated as an active electrode material for lithium-ion batteries. Diatom biosilica was obtained by cultivation of the selected diatom species under laboratory conditions. Several instrumental techniques (XRD, FTIR, Raman, SEM-EDX, TGA) were used to characterize the physicochemical properties of applied biosilica. It was evidenced that the prepared new composite material has a significant impact on the electrochemical properties of the electrode. The ratio 1:1 of biosilica and carbon black exhibited a specific capacity of 400 ± 9 mAh/g over 90 cycles. Such a ratio ensured proper electric contact between biosilica particles. The specificity of the faradaic process suggests that biosilica-based electrodes might be suitable in large-scale energy storage applications.

1. Introduction

Population growth in the world is a factor which causes an increase of electric energy consumption. Nowadays, electric energy is mainly produced in power plants or nuclear plants. Power plants utilize carbon to generate electricity in a combustion process with formation of huge amounts of carbon dioxide and water. Carbon dioxide is known as a greenhouse gas that traps heat in the atmosphere. As an effect of this climate change is observed [1].

In recent years it was decided that CO_2 emission should be reduced due to environmental reasons. There are other possibilities of generating electricity by utilizing an environmentally friendly way. Much attention is paid to use of cleaner renewable sources such as solar and wind energy. The problem with solar and wind energy is that they can be generated only during the daytime and when the wind is blowing, respectively. Another issue is that renewable energy should be stored in case of times with no sun (night) and no wind. Therefore, energy storage devices with a high energy density and a long-life cycle are needed. Lithium-ion batteries might be a possible choice due to the fact that lithium metal is the lightest and exhibits a theoretical capacity of 3860 mAh/g [2]. However, practical usage of metallic lithium anodes suffers from high reactivity of the lithium metal leading to reactivity with organic electrolytes and dendritic growth during subsequent charge-discharge cycles leading to explosion hazards [3,4]. Since intercalation of lithium ions into carbon was discovered in 1983 [5] commercial rechargeable batteries with negative electrodes based on carbon are in use from 1991 [6]. The theoretical capacity of a graphite electrode of stoichiometry LiC_6 is 372 mAh/g [2]. It is over 10 times lower in comparison with metallic lithium. Moreover, the graphite anode exhibits high capacity loss during the first lithium insertion. It is due to the formation of a solid electrolyte interphase (SEI) on the electrode. It is a protective film which prevents further negative electrode decomposition [7].

The current demand for energy leads to a search for batteries of better density, improved longevity and safety. Such storage systems are known as next-generation lithium batteries. Silicon is a material which exhibits a theoretical capacity of 3579 mAh/g in the form of $Li_{15}Si_4$ [8]. It is also one of the most abundant elements present on Earth in SiO_2 form. There is a possibility to use silica directly as an active component of the anode material [9]. The theoretical capacity of SiO_2 varies in the range from 749 mAh/g to 1965 mAh/g and depends on the mechanism [10]:

$$5SiO_2 + 4Li^+ + 4e^- \leftrightarrow 2Li_2Si_2O_5 + Si \quad (1)$$

$$4Si + 15Li^+ + 15e^- \leftrightarrow Li_{15}Si_4 \quad (2)$$

$$2SiO_2 + 4Li^+ + 4e^- \rightarrow Li_4SiO_4 + Si \quad (3)$$

$$2SiO_2 + 4Li^+ + 4e^- \rightarrow 2Li_2O + Si \quad (4)$$

Reactions (1)–(4) belong to a group of Faradaic processes taking part at an electrode. Reactions (1) and (2) are reversible, while reactions (3) and (4) are found to be irreversible, and affect the total capacity available for SiO_2 reduction. The Faradaic process involves a charge transfer reaction at the electrode. In other words, a redox reaction must occur in the system. The reaction between silica and the

* Corresponding author.
E-mail address: andnowak@pg.edu.pl (A.P. Nowak).

https://doi.org/10.1016/j.algal.2019.101538
Received 22 February 2019; Received in revised form 6 May 2019; Accepted 7 May 2019
Available online 16 May 2019

lithium ion fulfils these requirements.

According to Faraday's law, the specific charge capacity Q, which quantifies how much charge is stored per mass (m) of active material can be calculated as follow:

$$Q = \frac{n \cdot F \cdot 1000}{3600 \cdot M_{mol}}$$

where,

Q – specific capacity [mAh/g],
n – number of electrons involved in the reaction,
F – Faraday constant (96,485C/mol) and C = A·s,
M_{mol} = molar mass of host material [g/mol].

Thus, the theoretical specific capacity of $Li_{15}Si_4$ ($Li_{3.75}Si$) is 3579 mAh/g as $n = \frac{15}{4} = 3.75$ and $M_{mol} = 28.02$ g/mol.

There are a variety of silica forms among mineral natural resources from crystalline quartz combining minerals to amorphous opal silica hydrated forms [11]. The silica to be exploited in an electrode should be present as very small particulates uniformly spread inside electron conductors such as carbon [12,13] or copper [14]. The higher the ratio between the bulk volume to the real surface area of the electroactive material the better the practical charge capacity. Thus, the use of nanostructured materials is expected to solve not only the problem with silicon volume expansion under alloying (see reaction (6)) but also should provide better electrode capacity [15]. Many efforts and costs have been put into the development of technology for the production of nanomaterials applicable in electric energy storage and conversion [16]. The main disadvantage of synthetic nanomaterials production is their high energy consumption and the inevitably growing environmental safety risk. There are difficulties in large scale production, also unknown is the biocompatibility of novel nanostructures which is not justified for sustainable development and for environmental protection. Recently a novel source of 3-dimensional (3D) natural biosilica originated from single cell algae-diatoms has been demonstrated as an "emerging biomaterial for energy conversion and storage" [17]. Biosilica containing diatoms are a type of algae which can be found in oceans, seas, inland waters and soils of the world [18–20]. Algae take part in biomineralizations forming the silica frustule. Among the more general biomineralization processes, those involving silica are known as biosilification [21]. The diatom variety in nano and micromorphologies and patterns is available worldwide [22,23]. The search for the most suitable 3-D architecture is open for researchers. Biosilica, already tested as the precursor for Li-ion anode preparation, is available directly from mineral resources in the form of *i*) diatomic earth or from *ii*) marine biomass with diatom algae [24,25]. Besides, it is not the only field where diatom biosilica could be utilized [26–28]. There are many technologies in which diatom biosilica is commonly used [29]. Due to porous frustule architecture, diatomaceous earth is employed as a support for active chemical species in catalysis. Biosilica is also widely used in water treatment technologies. Novel possible applications of 3-D biosilica concerns delivery of pharmaceutics [30] and construction of nanodevices [31–33]. Moreover, the optical properties of diatom frustule are attractive for constructing optical sensors due to observed enhancement of the Raman signal (SERS) [34,35]. Biosilica possesses an ability to protect DNA from damage caused by UV radiation, and this phenomenon can flourish in future applications in solar energy harvesting devices [36].

This fascinating 3-D shaped micro- and nanoporous biosilica element can be obtained from diatomic earth or like in this study from cultivated microalgae species – diatoms. There are also other naturally existing species containing biosilica. Among them rice husks, processed chemically, are a source of nano silica powder [37]. Also porous synthetic silica is available from man-made procedures, however of lower complexity in morphology in comparison with the biomaterial. Methods for obtaining silica-based nanomaterials are usually high-energy consuming. Long-term milling in quartz brings about nanosilica in the laboratory scale [38]. However, such a method is not scalable. In other technological procedures, SiO_2, nanomaterials are obtained by hydrolysis of silicon organic compounds (e.g. tetraethoxysilane (TEOS)) [14]. Commercial production of this most prominent alkoxysilane requires more efforts undertaken in respect to economic and environmental aspects as was shown by Segovia-Hernández et al. [39]. It is very important to underline that by using natural biosilica of 3-D structures, one saves energy and chemicals needed to obtain organic derivatives of silicon and their further processing into porous SiO_2 structures. Nevertheless, one should take into account that microalgal biomass production is not a costless process. In general, the microalgal biomass is obtained in two-stage procedures: 1) harvesting and dewatering, followed by 2) extraction, fractionation and conversion. Recently, van Boxtel et al. showed that the economic costs are in the range from 0.5 to 2.0 €/kg algae with energy consumption up to 4.5 kWh/kg algae. These values might be reduced for closed cultivation systems to 0.1–0.6 €/kg algae and 0.1–0.7 kWh/kg algae for the operational and energy consumption costs, respectively [40].

Herein, we present 3D-structured diatom biosilica (*Pseudostaurosira trainorii*) as a negative electrode material for lithium-ion batteries. The diatom biosilica obtained under laboratory conditions by the cultivation of the selected species was taken to work as an electrode film. The utilization of biosilica-based electrodes for energy storage of high energy density and a long-life cycle was examined.

2. Materials and methods

2.1. Sample preparation

The diatom species *Pseudostaurosira trainorii* was provided by the Culture Collection of Baltic Algae, Institute of Oceanography, University of Gdansk, Poland. Diatom biosilica was fabricated by the cultivation of the selected diatom species under laboratory conditions using Erlenmeyer flasks with a Guillard's F/2 growth solution adjusted to pH 8.4 and containing silica ($Na_2SiO_3 \cdot 5H_2O$) at a concentration of 7 mg/L. The cultivation was carried out at a 12 h light/12 h darkness regime, aeration, and a constant temperature of 20 °C. Diatom cells were collected by filtration via Millipore 0.45 μm filters using a vacuum pump. The diatom biosilica was isolated from washed diatom cells using hydrogen peroxide (30% H_2O_2) to digest organic matter at 80 °C for 4 h, and hydrochloric acid (37% HCl) to dissolve calcium carbonates at the end of the hot hydrogen peroxide oxidation process. The obtained diatom biosilica was washed with distilled water and dried at 120 °C in air.

2.2. Characterization of biosilica with solid-state physics techniques

Scanning electron microscopy (SEM LEO 1430VP) equipped with an energy dispersive spectrometer (EDS, detector XFlash 4010 Bruker AXS) was used to study the morphology and the elemental composition of the cleaned diatom frustules. An FTIR spectrophotometer (FTIR ATR, Vertex 70, Bruker Optyc) equipped with a DLaTGS detector was used to determine structural bonds and functional groups of the biosilica. The FTIR spectrum was recorded by averaging 64 scans in the wave number range 200 cm^{-1} to 4000 cm^{-1} with a resolution of 4 cm^{-1}. X-ray powder diffraction (XRD) measurements were performed using an X'Pert Pro diffractometer with Cu-Kα radiation (λ = 0.1541 nm, 40 kV, 30 mA). The biosilica sample was scanned in the range between 5 and 120° 2θ with step sizes of 0.0167. Thermal analysis was carried out using a TGA–DTA Thermal Analysis Instruments SDT 2960 derivatograph in the temperature range 20–1000 °C. The analysis was conducted with a linear heating rate of 10 °C/min in a nitrogen gas flow.

EDX analysis was conducted for 1 replicate at three different spots. No important differences were noticed for XRD, FTIR and TGA measurements. Hence, we did not perform statistical analysis for those

solid-state physics techniques.

2.3. Preparation of electrode materials

The biosilica frustules originating from cultivated diatom biosilica were used as an active electrode material for electrochemical tests. Two electrode films were prepared from the slurry containing diatom biosilica (DB), carbon black (CB) (Super P, Timcal, Switzerland) and CMC (Sodium carboxymethyl cellulose, $M_w \sim 250{,}000$, Aldrich) with water as solvent, at a weight ratio of 1:1:1 (DB/CB 1:1) or 1:2:1 (DB/CB 1:2) on a copper current collector (Schlenk Metallfolien GmbH & Co KG, Germany). After that, the tape casting material was dried, cut from the tape and pressed (60 s with a load of 100 MPa), followed by drying under dynamic vacuum in an oven (Glass Oven B-585 Büchi, Germany) for 24 h at 90 °C. The drying process was performed to remove any traces of water adsorbed at the film electrode surface. The electrode materials were tested in a two-electrode Swagelok® cell with lithium foil (99.9%, 0.75 mm thickness, AlfaAesar) as the counter and reference electrode. LP 30 (Merck) was used as the electrolyte and glass fiber (Schleicher & Schüll, Germany) soaked with electrolyte as the separator. The cells were assembled in an argon-filled glove box (O_2 < 0.5 ppm and H_2O < 0.5 ppm) (MB-Labstar 1200/780, MBRAUN, Germany).

2.4. Electrochemical characterization of the electrode material

The battery tests of the samples were performed using the ATLAS 0961 MBI (Poland) multichannel battery testing system using different constant-current densities that were stable ± 1%. The cells were first charged with a current density of 20 mA/g. When the potential reached 0.002 V, the current direction was reversed and the cells were discharged to 3.0 V.

Cyclic voltammetry measurements (CV) were carried out on a PGSTAT204 (The Netherlands) galvanostat/potentiostat over the potential range 0.002–3 V vs. Li/Li^+ with a scanning rate of 100 μV/s. The electrode material was first reduced to reach the cut off voltage of 0.002 V followed by oxidation up to 3.0 V.

The experimental measurements were carried out with 3 replicates for each electrode material.

2.5. Statistical analysis

The results for galvanostatic tests are shown as the average for n = 3. All statistical analyses were performed using LibreOffice version 6.1.4.2(x64) for Windows.

3. Results and discussion

The X-ray diffraction patterns of the diatom biosilica (Fig. 1A) are characterized by a single intense broad peak at 15–35° 2θ (CuKα). An XRD pattern of this kind is specific for amorphous silica such as opal – A [41,42].

The scanning electron microphotographs (insert A-II, Fig. 1A) gave a view of the cleaned diatom frustules. The valves of the frustules shaped like an oval saucer with an average diameter of 4–5 μm are very well preserved and uniform. The silica walls of the valves are perforated by a network of parallel rows of oval pores with sizes in the range of 150–200 nm with gaps between separated pore rows near 450 nm and the space between the individual pores in the rows of about 130 nm, as it has been already reported in [43]. The elementary composition of the diatom biosilica obtained using SEM-EDX is presented in the insert table in Fig. 1a. These data demonstrated that silicon and oxygen are the basic elements of the biosilica with the atomic O:Si ratio as 1.29:1. The amorphous nature of the biosilica is also confirmed and indicates the relatively high content of Si-OH groups in the biosilica structure.

The results of FTIR-ATR spectroscopy are shown in Fig. 1B. The most intensive band centered at 1062 cm^{-1} is attributed to asymmetric stretching vibrations of Si–O–Si bonds in the biosilica structure. The band appearing at 943 cm^{-1} is reflected by the asymmetric stretching vibration of Si—O bonds in silanol groups Si–O–H and the band at 797 cm^{-1} is caused by symmetric bending vibrations of Si–O–Si bonds [44,45]. The presence of an intense absorption peak centered at 447 cm^{-1} is assigned to bending vibrations of Si—O bonds in siloxane groups Si–O–Si [24,46]. The broad band at around 3650–3000 cm^{-1} is related to stretching vibrations of O—H bonds in silanol groups, as well as in hydrogen bonded molecular water. The band at 1626 cm^{-1} is due to bending vibrations of H–O–H bonds of bound molecular water [47].

The thermogravimetric analysis (TGA) curves of the biosilica are shown in Fig. 1C. Three distinct stages of weight loss during heating may be identified for the biosilica. At the first stage (25–126 °C) weight loss of biosilica of 5.5% is due to loss of weakly hydrogen-bonded water molecules (dehydration process). This stage is accompanied by a 126 °C DTG peak at 59 °C and an endothermic effect on the DTA curve. A weight loss of 6% observed during the second stage at the temperature interval 257–675 °C may be attributed to the release of water by the condensation product of silanol groups (dehydroxylation process). The third stage with 1.3% weight loss appears in the temperature interval 675–901 °C. This phase may be referred mainly to condensation and removal from biosilica of internal isolated hydroxyl groups (the dehydroxylation process).

Cyclic voltammetry (cv) measurements for ZO/CB 1:1 and ZO/CB 1:2 were investigated in a half cell configuration at 100 μV/s in the potential range from 0.002 V to 3.0 V. The shape of cv curves recorded for both electrode materials was similar, hence the cv curve for only ZO/CB 1:1 has been shown, see Fig. 2.

During the first charging process one may see a cathodic maximum at E = 0.70 V. This peak maximum is not present in subsequent cycles, and is attributed to material reduction coupled with solid electrolyte interphase (SEI) formation at the electrode [10,48]. One may also see broad anodic and cathodic plateaus at 0.89 V and 0.83 V, respectively. The observed redox couple activity at E = 0.86 V might be attributed to the reversible reaction between SiO_2 and Li^+ ions with $Li_2Si_2O_5$ and Si formation, according to reaction (1). However, Yang et al. claimed that the origin of such electrode activity was due to irreversible reactions of

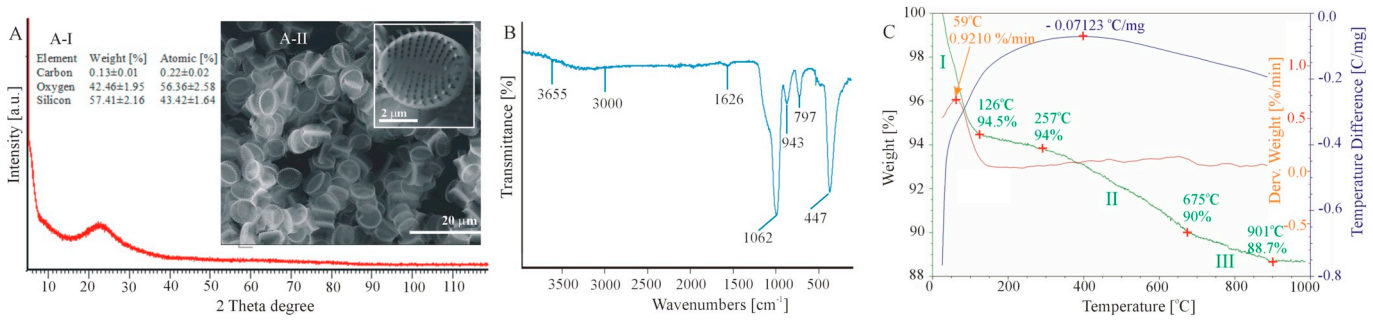

Fig. 1. XRD pattern (A), elemental composition (A-I), scanning electron microscopy image (A-II), FTIR-ATR spectrum (B) and TGA curves (C) of the diatom biosilica.

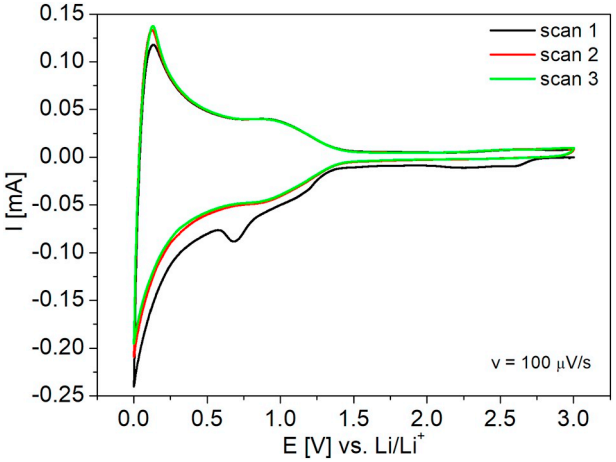

Fig. 2. The cv curve of the DB/CB 1:1 electrode in 1 M $LiPF_6$ in EC/DMC. Potential range 0.002–3 V. The sweep rate v = 100 μV/s.

inert materials within the electrode [49]. In the studied case we excluded that possibility as the cv curves for the 2nd and 3rd cycles overlapped, confirming reversible reactions taking place. Further reduction of the electrode material led to alloy formation Li_xSi.

The specific capacity determination was performed with the use of galvanostatic charge/discharge tests. Fig. 3 shows the capacity change vs the cycle number and applied current density. In the experiment, the current density equal to 20 mA/g corresponds to a rate of C/40 (battery charging at a rate of C/40 will deliver its nominal capacity in 40 h). Such a long time was chosen due to a low value of the lithium ion diffusion coefficient in silicon [50] and silica [51].

The summarized results for each electrode material are gathered in Table 1.

The noticeable capacity drop between the first and second cycle is attributed to the solid electrolyte interphase (SEI) formation, as it was also evidenced for cv tests. One may see that even for subsequence cycles (2–5 at a current density equal to 20 mA/g) charge capacities are higher than discharge capacities. We assumed this phenomenon was due to irreversible reactions between silica particles and lithium ions during the reduction process [52]:

$$2SiO_2 + 4Li^+ + 4e^- \rightarrow Li_4SiO_4 + Si \quad (3)$$

$$SiO_2 + 4Li^+ + 4e^- \rightarrow 2Li_2O + Si \quad (4)$$

It was already shown that such reactions occur during lithiation of SiO_x nanowires with Li_2O, as well as Li_4SiO_4 formation [53]. The reaction between Li^+ and SiO_2 takes place on the outer layer of SiO_2 and therefore several subsequence cycles were needed to fully convert silica into lithium oxide and lithium orthosilicate. The average discharge capacity after the first 5 cycles was 407 ± 2 mAh/g for DB/CB 1:1 and 370 ± 10 mAh/g for DB/CB 1:2, which was higher than for the graphite electrode. Further galvanostatic polarization tests at a current density of 100 mA/g showed a capacity drop to 295 ± 2 mAh/g and 190 ± 10 mAh/g for DB/CB 1:1 and DB/CB 1:2, respectively. It was about 112 mAh/g less for the former and over 170 mAh/g for the latter, in comparison with the discharge capacity measured at 20 mA/g.

Subsequent cycles at j = 500 mA/g gave average specific capacities of 75 ± 1 mAh/g for DB/CB 1:1 and 42 ± 1 DB/CB for 1:1 electrode materials. Such a drastic drop in the specific capacity value evidenced that the material is not suitable for the fast charging/discharging process. Lithium ion diffusion within the bulk electrode is the slowest process and limits the utilization of the DB-based electrode for high power application.

After applying an initial value of current density (20 mA/g) DB/CB 1:1 exhibited a specific discharge capacity of ~409 ± 4 mAh/g, as was measured previously. It showed that higher current densities did not affect the capacity of the electrode material, and evidenced that lithium ion intercalation into a host material is a reversible process. The coulombic efficiency was above 98% after 90 cycles. However, electrochemical performance of the electrode at the DB/CB 1:2 ratio was much worse. Carbon black (CB) is known to be a good electron conductor but a very poor ion conductor. Lithium electrosorption into CB is limited, and thus its contribution to reversible capacity can be neglected [54]. Hence, the amount of lithium cations delivered to silica is not sufficient for an efficient faradaic process (see Eqs. (1)–(4)) and one may expect that the main process is limited to the SEI growth. The material seemed to be degraded during cycling. It is very likely that excess of conducting material might have caused faster ageing of the electrode material during cycling, as it is observed for carbonaceous anodes [55]. It is very likely that in the studied case continuous SEI formation occurred which led to volume changes and contact loss of active material particles. One may see cracks appearing on the surface of the DB/CB 1:2 electrode material after cycles, see Fig. 4. The presence of cracks leads to a capacity fade seen as a decrease of specific capacity of the electrode mentioned above.

4. Conclusion

Diatom biosilica, obtained from laboratory-cultivated diatom algae, has been investigated as an anode electrode material for lithium-ion

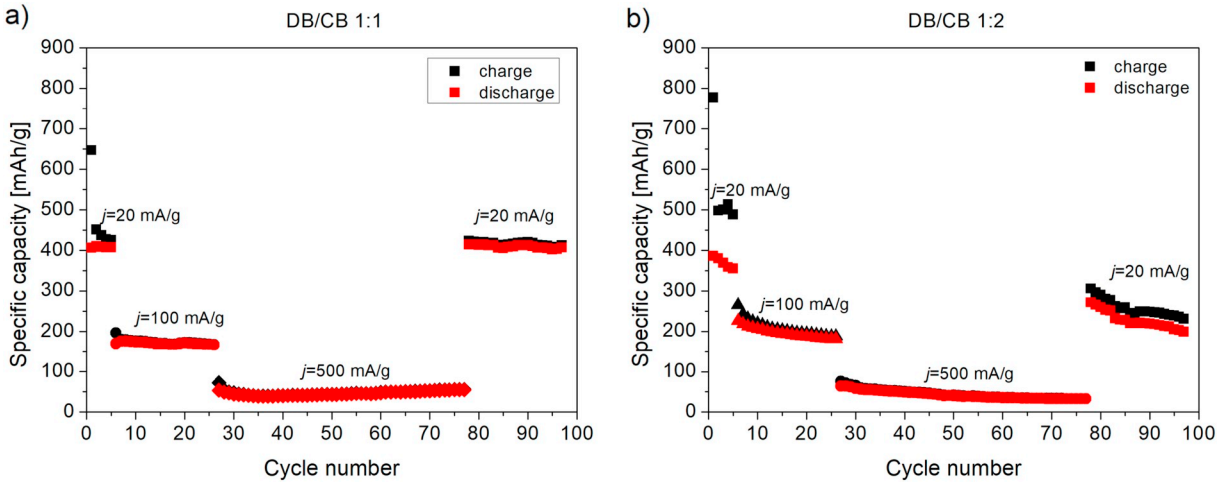

Fig. 3. The capacity vs. cycle number of diatom biosilica-based electrodes at different C-rates for a) DB/CB ratio of 1:1 and b) DB/CB ratio of 1:2. Data are shown as the average of replication of each cycle for the specified electrode material, n = 3.

Table 1
The average of specific capacity as the function of applied current.

Electrode material	Current density [mA/g]							
	20		100		500		20	
	Charge [mA/g]	Discharge [mA/g]	Charge [mA/g]	Discharge [mA/g]	Charge [mA/g]	Discharge [mA/g]	Charge [mA/g]	Discharge [mA/g]
DB/CB 1:1[a]	470 ± 80	407 ± 2	296 ± 3	295 ± 2	75 ± 1	75 ± 1	416 ± 4	409 ± 4
DB/CB 1:2[a]	500 ± 100	370 ± 10	207 ± 20	190 ± 10	42 ± 9	42 ± 9	260 ± 30	230 ± 30

[a] Results are presented as the average ± SD (n = 3) of measurements at each current density taken from data from Fig. 3.

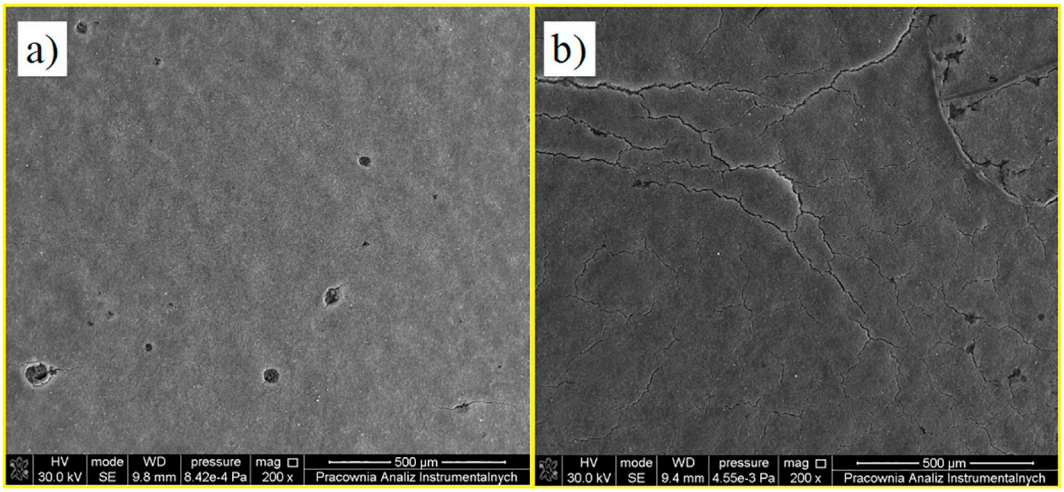

Fig. 4. The SEM images of DB/CB electrode material 1:2 a) before and b) after polarization tests.

batteries. Diatom biosilica is presented as very well preserved and uniform diatom frustules with a three-dimensional structure perforated by a periodic pore network and composed of amorphous silica like opal-A. High thermostability, a relatively high content of hydrogen bonded water in the structure and strong FTIR scattering are characteristic features for biosilica used. Electrochemical tests evidenced that the ratio of DB to carbon black (CB) affected the specific capacity of the electrode material. The DB/CB material of ratio 1:1 turned out to exhibit the best properties with a specific capacity of ~409 ± 4 mAh/g for a current density equal to 20 mA/g after over 90 charge/discharge cycles. The specific capacity for higher current densities (500 mA/g) was below 100 mAh/g. It showed that the lithium-ion faradaic reaction with silica is a slow process and such a kind of electrode material might be rather more suitable for large-scale energy storage than for electric vehicles. We have demonstrated that the use of a naturally occurring biosilica, available globally, allows an increase of the charge capacity of the negative electrode, compared to the commonly used graphite.

Acknowledgement

This work was supported by the Ministerstwo Nauki i Szkolnictwa Wyższego (DS no. 032406).

Declaration of author contributions

Andrzej P. Nowak – designed and conducted the electrochemical experiments, writing and critical revision of the article as well as data analysis and interpretation.

Myroslav Sprynskyy – cultivation of the biosilica, characterization of the biosilica with solid-state physics techniques, writing the article, as well as data analysis and interpretation.

Weronika Brzozowska – collection of experimental data and data interpretation.

Anna Lisowska-Oleksiak – initiator of the research, drafting the article and critical revision. Final approval of the article.

The authors declare no conflict of interest, informed consent, human or animal rights applicable.

References

[1] S. Solomon, G.-K. Plattner, R. Knutti, P. Friedlingstein, P. Natl, Acad. Sci. USA 106 (2009) 1704–1709.
[2] M. Wakihara, Y. Yamamoto, O. Yamamoto, Lithium Ion Batteries Fundamentals, and Performance, Kodansha, Willey-VCH, Tokyo, 1998.
[3] R.A. Huggins, Lithium alloy negative electrodes, J. Power Sources 81-82 (1999) 13–19.
[4] J.-M. Tarascon, M. Armand, Issues and challenges facing rechargeable lithium batteries, Nature 414 (2001) 359–367.
[5] R. Yazami, Ph. Touzain, A reversible graphite-lithium negative electrode for electrochemical generators, J. Power Sources 9 (1983) 365–371.
[6] T. Nagaura, K. Tozawa, Lithium ion rechargeable battery, Prog. Batteries Solar Cells 9 (1990) 209–217.
[7] E. Peled, The electrochemical behavior of alkali and alkaline earth metals in non-aqueous battery systems—the solid electrolyte interphase model, J. Electrochem. Soc. 126 (1979) 2047–2051.
[8] A.P. Nowak, Composites of tin oxide and different carbonaceous materials as negative electrodes in lithium-ion batteries, J. Solid State Electrochem., DOI: https://doi.org/10.1007/s10008-018-3942-y.
[9] Q. Sun, B. Zhang, Z.-W. Fu, Lithium electrochemistry of SiO_2 thin film electrode for lithium-ion batteries, Appl. Surf. Sci. 254 (2008) 3774–3779.
[10] N. Yan, F. Wang, H. Zhong, Y. Li, Y. Wang, L. Hu, Q. Chen, Hollow porous SiO_2 nanocubes towards high-performance anodes for lithium-ion batteries, Sci. Rep. 3 (2013) 1568–1574.
[11] A.F. Rogers, Natural history of the silica minerals, Am. Mineral. 13 (1928) 73–92.
[12] Z. Favors, W. Wang, H.H. Bay, Z. Mutlu, K. Ahmed, C. Liu, M. Ozkan, C.S. Ozkan, Scalable synthesis of nano-silicon from beach sand for long cycle life Li-ion batteries, Sci. Rep. 4 (5623) (2014) 1–6.
[13] M.-S. Wang, Z.-Q. Wang, R. Jia, Y. Yang, F.-Y. Zhu, Z.-L. Yang, Y. Huang, X. Li, W. Xu, Facile electrostatic self-assembly of silicon/reduced graphene oxide porous composite by silica assist as high performance anode for Li-ion battery, Appl. Surf. Sci. 456 (2018) 379–389.
[14] B. Wicikowska, A.P. Nowak, Konrad Trzciński, A. Lisowska-Oleksiak, Electrochemical activity of electrode material consisting of porous copper and silica aerogel, Procedia Engineer 98 (2014) 42–45.

[15] A.S. Aricò, P. Bruce, B. Scrosati, J.-M. Tarascon, W. van Schalkwijk, Nanostructured materials for advanced energy conversion and storage devices, Nat. Mater. 4 (2005) 366–377.
[16] S.C. Nagpure, B. Bhushan, Nanomaterials for electrical energy storage devices, in: B. Bhushan (Ed.), Encyclopedia of Nanotechnology, Springer, Dordrecht, 2016.
[17] X.W. Sun, Y.X. Zhang, D. Losic, Diatom silica, an emerging biomaterial for energy conversion and storage, J. Mater. Chem. A 5 (2017) 8847–8859.
[18] M. Cegłowska, A. Toruńska-Sitarz, G. Kowalewska, H. Mazur-Marzec, Specific and genetic markers revealed a thousands-year presence of toxic Nodularia spumigena in the Baltic Sea, Mar. Drugs 16 (2018) 1–11, https://doi.org/10.3390/md16040116 (116).
[19] T. Jóźwiak, H. Mazur-Marzec, M. Pliński, Cyanobacterial blooms in the Gulf of Gdańsk (southern Baltic): the main effect of eutrophication, Oceanol. Hydrobiol. St. 37 (2008) 115–121.
[20] M. De Stefano, L. De Stefano, Nanostructures in diatom frustules: functional morphology of valvocopulae in Cocconeidacean monoraphid taxa, J. Nanosci. Nanotechnol. 5 (2005) 15–24.
[21] M. Wysokowski, T. Jesionowski, H. Ehrlich, Biosilica as a source for inspiration in biological materials science, Am. Mineral. 103 (2018) 665–691.
[22] M. Gross, The mysterious of the diatoms, Curr. Biol. 22 (2012) R581–R585.
[23] E. De Tommasi, J. Gielis, A. Rogato, Diatom frustule morphogenesis and function: a multidisciplinary survey, Mar. Genom. 35 (2017) 1–18.
[24] A. Lisowska-Oleksiak, A.P. Nowak, B. Wicikowska, Aquatic biomass containing porous silica as an anode for lithium ion batteries, RSC Adv. 4 (2014) 40439–40443.
[25] J. Entwistle, A. Rennie, S. Patwardhan, A review of magnesiothermic reduction of silica to porous silicon for lithium-ion battery applications and beyond, J. Mater. Chem. A 6 (2018) 18344–18356.
[26] J. Rüger, N. Unger, I.W. Schie, E. Brunner, J. Popp, C. Kraff, Assessment of growth phases of the diatom Ditylum brightwellii by FT-IR and Raman spectroscopy, Algal Res. 19 (2016) 246–252.
[27] A. Ozkan, G.L. Rorrer, Effects of CO_2 delivery on fatty acid and chitin nanofiber production during photobioreactor cultivation of the marine diatom Cyclotella sp, Algal Res. 26 (2017) 422–430.
[28] N. Pytlik, J. Kaden, M. Finger, J. Naumann, S. Wanke, S. Machill, E. Brunner, Biological synthesis of gold nanoparticles by the diatom Stephanopyxis turris and in vivo SERS analyses, Algal Res. 28 (2017) 9–15.
[29] J. Seckbach, P. Kociolek, The Diatom World, Springer, Netherlands, 2011.
[30] N.I. Vazquez, Z. Gonzalez, B. Ferrari, Y. Castro, Synthesis of mesoporous silica nanoparticles by sol-gel as nanocontainer for future drug delivery applications, Bol. Soc. Esp. Ceram. V 56 (2017) 139–145.
[31] I. Rea, M. Terracciano, S. Chandrasekaran, N. Voelcker, P. Dardano, N.M. Martucci, A. Lamberti, L. De Stefano, Bioengineered silicon diatoms: adding photonic features to a nanostructured semiconductive material for biomolecular sensing, Nanoscale Res. Lett. 11 (1–9) (2016) 405.
[32] I. Rea, M. Terracciano, L. De Stefano, Synthetic vs natural: diatom bioderived porous materials for next generation of healthcare nanodevices, Adv. Healthcare Mater. 6 (1601125) (2017) 1–12.
[33] M, Terracciano, L. De Stefano, I. Rea, Diatoms green nanotechnology for biosilica-based drug delivery systems, Pharmaceutics, 10 (2018) 242(1–15).
[34] L. De Stefano, M. De Stefano, E. De Tommasi, I. Rea, I. Rendina, A natural source of porous biosilica for nanotech applications: the diatoms microalgae, Phys. Status Solidi C 8 (2011) 1820–1825.
[35] M. Pannico, I. Rea, S. Chandrasekaran, P. Musto, N.H. Voelcker, L. De Stefano, Electroless gold-modified diatoms as surface-enhanced Raman scattering supports, Nanoscale Res. Lett. 11 (1–6) (2016) 315.
[36] L. De Stefano, P. Maddalena, L. Moretti, I. Rea, I. Rendina, E. De Tommasi, V. Mocella, M. De Stefano, Nano-biosilica from marine diatoms: a brand new material for photonic applications, Superlattice. Microst. 46 (2009) 84–89.
[37] R. Yuvakkumar, V. Elango, V. Rajendran, N. Kannan, High-purity nano silica powder from rice husk using a simple chemical method, J. Exp. Nanosci. 9 (2014) 272–281.
[38] W.-S. Chang, C.-M. Park, J.-H. Kim, Y.-U. Kim, G. Jeong, H.-J. Sohn, Quartz (SiO_2): a new energy storage anode material for Li-ion batteries, Energy Environ. Sci. 5 (2012) 6895–6899.
[39] J.P. Palma-Barrera, E. Sanchez-Ramírez, C. Ramírez-Marquez, J.A. Cervantes-Jauregui, J.G. Segovia-Hernandez, Reactive distillation column design for tetraethoxysilane (TEOS) production. Part II: dynamic properties and inherent safety, Ind. Eng. Chem. Res. 58 (2019) 259–275.
[40] F. Fasaei, J.H. Bitter, P.M. Slegers, A.J.B. van Boxtel, Techno-economic evaluation of microalgae harvesting and dewatering systems, Algal Res. 31 (2018) 246–252.
[41] J.M. Elzea, S.B. Rice, TEM and X-ray diffraction evidence for cristobalite and tridymite stacking sequences in opal, Clay Clay Miner. 44 (1996) 492–500.
[42] J. Eckert, O. Gourdon, D.E. Jacob, C. Meral, P.J.M. Monteir, S.C. Vogel, R. Wirth, H.-R. Wenk, Ordering of water in opals with different microstructures, Eur. J. Mineral. 27 (2015) 203–213.
[43] M. Sprynskyy, P. Pomastowski, M. Hornowska, A. Król, K. Rafińska, B. Buszewski, Naturally organic functionalized 3D biosilica from diatom microalgae, Mater. Des. 132 (2017) 22–29.
[44] V.C. Farmer, The Infrared Spectra of Minerals, Mineralogical Society, London, UK, 1974.
[45] M. Hernández-Ortiz, G. Hernández-Padrón, R. Bernal, C. Cruz-Vázquez, V.M. Castaño, Nanocrystalline mimetic opals: synthesis and comparative characterization vs. natural stones, Int. J. Basic Appl. Sci. 4 (2015) 238–243.
[46] S. Music, N. Filipovic-Vincekovic, L. Sekovanic, Precipitation of amorphous SiO_2 particles and their properties, Brazilian J. Chem. Eng. 28 (2011) 89–94.
[47] W. Jiang, S. Luo, P. Liu, X. Deng, Y. Jing, C. Bai, J. Li, Purification of biosilica from living diatoms by a two-step acid cleaning and baking method, J. Appl. Phycol. 26 (2014) 1511–1518.
[48] A.P. Nowak, A. Lisowska-Oleksiak, K. Siuzdak, M. Sawczak, M. Gazda, J. Karczewski, G. Trykowski, Tin oxide nanoparticles from laser ablation encapsulated in a carbonaceous matrix – a negative electrode in lithium-ion battery applications, RSC Adv. 5 (2015) 84321–84327.
[49] J. Yang, Y. Takeda, N. Imanishi, C. Capiglia, J.Y. Xie, O. Yamamoto, SiO_x-based anodes for secondary lithium batteries, Solid State Ionics 152 (2002) 125–129.
[50] N. Ding, J. Xu, Y.X. Yao, G. Wegner, X. Fang, C.H. Chen, Determination of the diffusion coefficient of lithium ions in nano-Si, Solid State Ionics 180 (2009) 222–225.
[51] A. Ostadhossein, S.-Y. Kim, E.D. Cubuk, Y. Qi, A.C.T. van Duin, Atomic insight into the lithium storage and diffusion mechanism of SiO_2/Al_2O_3 electrodes of lithium ion batteries: ReaxFF reactive force field modeling, J. Physical Chem. A 120 (2016) 2114–2127.
[52] Y. Wang, K. Xie, X. Guo, W. Zhou, G. Song, S. Cheng, Mesoporous silica nanoparticles as high performance anode materials for lithium-ion batteries, New J. Chem. 40 (2016) 8202–8205.
[53] H. Jung, B.C. Yeo, K.-R. Lee, S.S. Han, Atomistics of the lithiation of oxidized silicon (SiO_x) nanowires in reactive molecular dynamics simulations, PCCP 18 (2016) 32078–32086.
[54] D.A. Stevens, J.R. Dahn, The mechanisms of lithium and sodium insertion in carbon materials, J. Electrochem. Soc. 148 (2001) A803–A811.
[55] J. Vetter, P. Novak, M.R. Wagner, C. Veit, K.-C. Mller, J.O. Besenhard, M. Winter, M. Wohlfahrt-Mehrens, C. Vogler, A. Hammouche, Ageing mechanisms in lithium-ion batteries, J. Power Sources 147 (2005) 269–281.